PLASMA CONTROL OF VORTEX FLOW ON A DELTA WING AT HIGH ANGLES OF ATTACK

Alexey D. Budovskiy[1], Andrei A. Sidorenko, Anatoly A. Maslov,
Boris V. Postnikov, Boris Yu. Zanin, Ilya D. Zverkov and Victor V. Kozlov –
Khristianovich Institute of Theoretical and Applied Mechanics, Siberian Division of the Russian Academy of Sciences, Novosibirsk, RUSSIA

Abstract

The flow over a delta wing at high angles of attack is characterized by the presence of two large–scale primary vortices on the leeward side of the wing. These vortices contribute substantially to lift production at high angles of attack. Therefore, vortex breakdown, which can be induced by unfavorable pressure gradient or free-stream disturbances, can lead to an abrupt decrease in lift and to the emergence of a roll moment. Thus, the possibility of vortex flow control can be very useful. The problem of vortex flow control is investigated experimentally under subsonic flow parameters. A dielectric barrier discharge (DBD) is used as an active control actuator. The data obtained by means of oil–flow and smoke flow visualization and surface pressure measurements show that the DBD can provoke early vortex bursting. Under certain conditions, flow excitation by a DBD actuator is found to result in vortex stabilization.

Introduction

The main feature of the flow on the leeward side of a delta wing at high angles of attack is the formation of two primary large-scale vortices (Fig. 1). Each vortex is able to generate a low-pressure region on the upper surface of the wing and create additional lift. The contribution of the vortex-induced lift to the total lift increases with increasing angle of attack and sweep angle of the delta wing and can reach up to half of the total lift at high angles of attack [1]. Therefore, the ability to manipulate and ultimately control vortex flow over a delta wing is of vital importance, because these vortices mainly determine aerodynamics of such wings at high angles of attack.

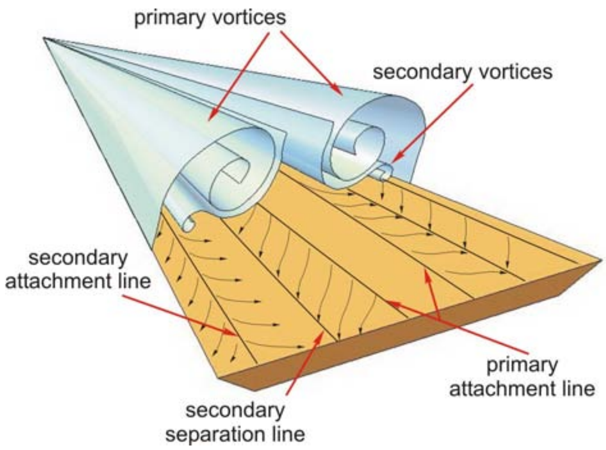

Fig. 1 Flow topology on delta wing at high angle of attack

The control strategy in this study was mainly focused on changing the vortex breakdown position, because this is the reason that makes the vortex lose its ability to create additional lift. The vortex breakdown phenomenon is caused by two main factors. The first one is an unfavorable pressure gradient, which is not that harmful. It is always present at the trailing edge of the wing and becomes gradually enhanced with increasing angle of attack. Therefore, the influence of this factor on vortex breakdown is fairly predictable. The second factor is the sensitivity of vortex flow to free-stream disturbances [2]. This factor is more dangerous as it can lead to a sudden decrease in lift and, moreover, to the emergence of a roll moment.

The paper deals with a new application of the dielectric barrier discharge (DBD) to vortex flow control on delta wings. This type of flow-control devices was proposed by Roth and Wilkinson [3], and it is well known to introduce desired periodic disturbances due to periodic flow acceleration in the boundary-layer region, as well as acoustic disturbances [4-5]. These features allow the DBD to be used for vortex breakdown control.

[1] budovsky@itam.nsc.ru

Experimental Setup

Wind Tunnel

The experiments were conducted at ITAM in a T-324 low-turbulence subsonic wind tunnel in the range of velocities of 3 to 33 m/s. The wind tunnel has a 1m × 1m × 4m square test section. The turbulence intensity *Tu* = 0.04% is sufficiently low, which facilitates extrapolation of wind-tunnel data to flight conditions and allows the influence of DBD-induced disturbances on vortex breakdown phenomenon to be studied.

Experimental Model

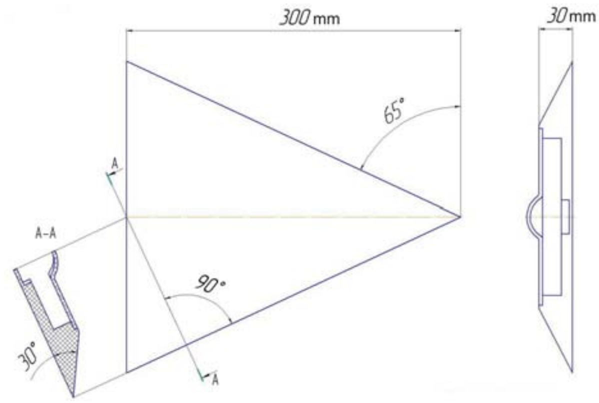

Fig. 2 Sketch of the delta wing model

Available publications on vortex breakdown on delta wings with a sharp leading edge under subsonic flow conditions show that vortex bursting occurs at certain critical angle of attack, which depends on the aspect ratio of the wing and does not depend on the Reynolds number. With allowance for the test-section geometry and the blockage ratio, an experimental model was prepared for wind-tunnel experiments. It is a delta wing with a leading edge sweep angle χ = 65°, chord length c = 300 mm, aspect ratio AR = 1.865, and thickness b = 30 m (Fig. 2). The leading edges of the delta wing are bevelled to 30°. The model is made of a dielectric material (Plexiglas). The delta wing was installed in the wind-tunnel test section on the sting of the mechanism for varying the angle of attack (α-variation mechanism) so the angle of attack could be varied in the range 0 ÷ 45°.

DBD Actuators and High Voltage Equipment

Design of DBD actuators is similar to that used in most studies dealing with DBD flow control [6-7] (see Fig. 3). The DBD electrodes are made of a 50 μm thick adhesive aluminum film. The encapsulated electrode is approximately 7 mm wide; the exposed electrode (also 7 mm wide) is glued with 1-mm overlapping. The barrier is made of three layers of a PVC adhesive film with the overall thickness of 240 μm. DBD actuators can be placed at various places on the model surface.

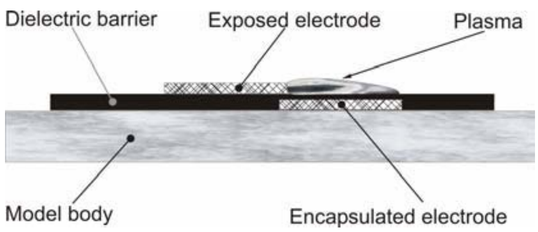

Fig. 3 Sketch of the plasma actuator

The DBD power supply (High Voltage Generator) used in the experiments was the same as that used in our earlier investigations [8]. The HVG was optimized for effective operation (internal loss of 5-7%) in the frequency range 0.5 ÷ 5 kHz. An example of measured high voltage and current in 1600-Hz pulses is shown in Fig. 4 The actuator was powered by AC voltage with a square waveform, and some secondary oscillations were observed during each half-period corresponding to self-induced oscillations of the HVG+DBD system. It can be seen that main plasma discharge appears at the beginning of the square pulse (seen as a series of

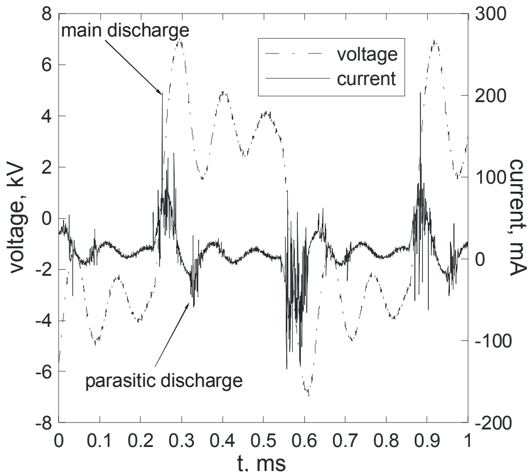

Fig. 4 Voltage and current pulses on the actuator (f = 1.6 kHz)

current spikes). A parasitic discharge of lower intensity is formed at the beginning of secondary pulses.

Measurement Techniques

Pressure measurement system

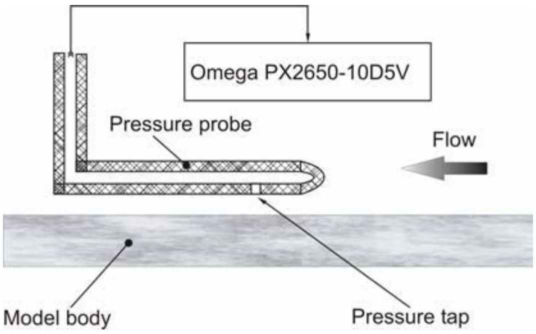

Fig. 5 Scheme of the pressure measurement system

Instead of the traditional surface pressure measurement technique with pressure taps and numerous sensors, an alternative method was used to reach a better space resolution on the entire surface of the model. The pressure distribution on the leeward side of the model was measured by a surface pressure probe made of stainless steel tube 0.8 mm in diameter. The pressure tap hole of the probe was perpendicular to the wing surface and was located in the near-wall region to measure the near-wall pressure (see Fig. 5). The probe was connected with an Omega PX2650-10D5V differential pressure gage (differential pressure transducer with a range of 0 to 10 inch-H_2O with a 0.2-5.2 Volt output), and the pressure was measured as the difference between the total pressures p_0 measured by a Pitot tube placed in the flow upstream of the wing and by the above-described probe. The pressure coefficient was obtained as

$$C_p = (p - p_0)/q + 1$$

The probe was moved along the surface by means of a three-component traversing gear. The accuracy of pressure measurements by such a probe was estimated in a separate test in comparison with the traditional pressure tap technique and was found to be about 5% for the present flow conditions [9].

Flow visualization

To get an idea about the mean flow and observe vortex evolution with increasing angle of attack, oil-flow and smoke flow visualization was used in the experiments. In the tests we used mixture of fluorescent die and kerosene brushed on the model surface, strokes were oriented across the main flow direction. The model was exposed in the flow until complete evaporation of kerosene and then the model was photographed. To increase of the image contract the model surface was painted in black color.

Smoke flow visualization was performed by the laser sheet method, as shown in Fig. 6. The laser sheet illuminated the flow in the plane perpendicular to the model surface. The smoke is injected far upstream of the model to minimize the possible influence on the flow. Video recording of visualization is performed by means of the camera installed on the pylon downstream of the model. To study the vortex flow pattern in various sections along the wing chord, a scanning laser sheet method was applied. In other words, the laser sheet was gradually moved from the wing tip to the trailing edge during the experiment.

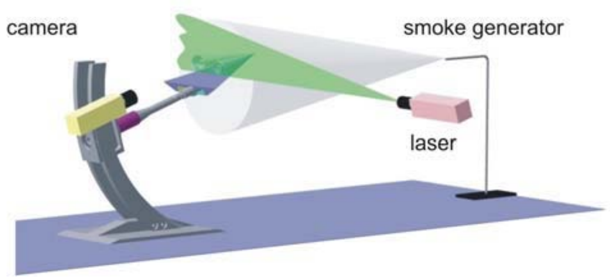

Fig. 6 Smoke flow visualization scheme

2D velocity measurements by PIV

The velocity measurements have been done by means of PIV system “POLIS” designed by Institute of Thermal Physics SB RAS. The system provides the following capabilities: laser energy per pulse – 70 mJ, pulse repetition rate – 8 Hz, size of image –1392x1040 pixels, resolution –12 bit.

The experiments were done using one camera installed on the pylon downstream of the model in such a way that plane of measurements was always normal to the model surface. The experimental setup is similar to one used for laser sheet visualization and presented in Fig. 6. Here high resolution CCD camera was used instead of analog video camera used in the smoke flow visualization test. To measure velocity distributions the whole contour of wind tunnel was seeded by smoke particles. Smoke concentration was sufficient to get contrast images of the smoke particles in the laser sheet.

Experimental Results

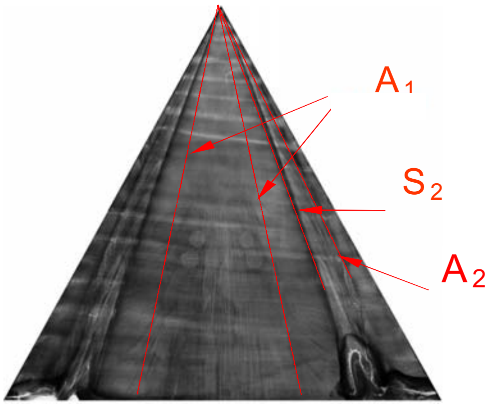

Fig. 7 Oil-flow visualization print
(α = 15°, U_∞=12 m/s)

DBD-assisted vortex breakdown control was studied in range of chord-based Reynolds numbers $0.14 \div 0.25 \cdot 10^6$. Series of preliminary tests were performed without DBD actuators. Oil-flow visualization and smoke flow visualization by means of the laser sheet were used to get an idea about the mean flow over the delta wing and its evolution with increasing angle of attack.

Oil-flow visualization gives us an opportunity to observe such features of the flow as attachment and separation lines. Smoke flow visualization assists in identifying the vortex location and provides an idea about the vortex pattern. A comparison of data obtained by these two techniques contributes to more detailed understanding of the flow structure over the delta wing.

It can be seen from Fig. 7 that a separated flow configuration with at least two vortices is formed on the leeward side of the delta wing at α = 15°. An analysis of surface streamlines allows us to see the primary vortex attachment line (A_1), as well as the secondary vortex separation and attachment lines (S_2 and A_2, respectively).

Oil-flow prints combined with smoke visualization for several sections are shown in Fig. 8 for two different angles of attack corresponding to different flow regimes. The data obtained show that the position of the vortex breakdown point gradually moves upstream to the wing tip with increasing angle of attack. For α smaller than 15°, vortex breakdown occur somewhere downstream from the model trailing edge. When the angle of attack reaches 15°, the right vortex breakdown point crosses the wing trailing edge, while the left vortex demonstrates the absence of breakdown. This tendency was observed in all the tests and could be probably attributed to inaccuracy in model positioning. It can also be noted from Fig. 8a that the secondary vortex separation lines (S_2 see Fig. 7) are slightly curved toward the wing centerline for angles of attack smaller than or equal to 15°. A further increase in α makes the vortex breakdown point move further upstream to the wing tip. It is worth noting that the line S_2 begins to bend toward the leading edge at this moment. The kink originates at α=17° and moves

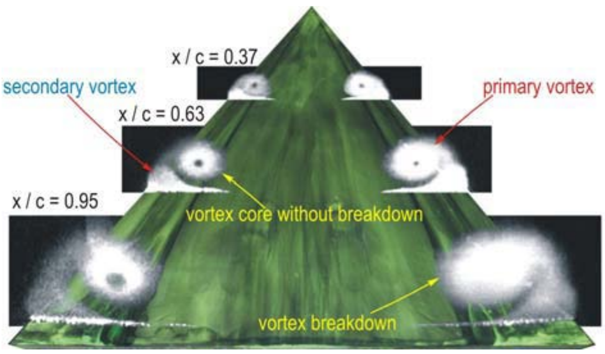

a) α = 15°

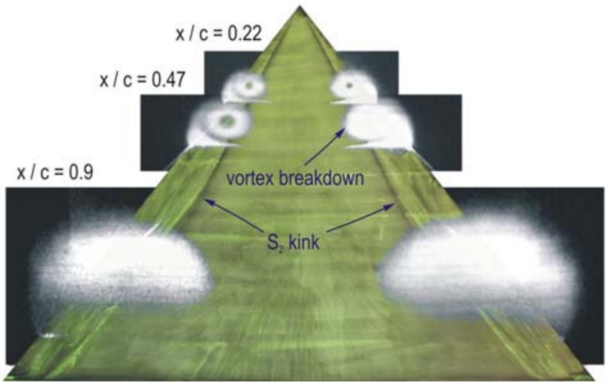

b) α = 22°

Fig. 8 Oil & Smoke flow visualization (U_∞= 12 m/s) together with the vortex breakdown point further upstream toward the wing tip with increasing α (Fig. 8b).

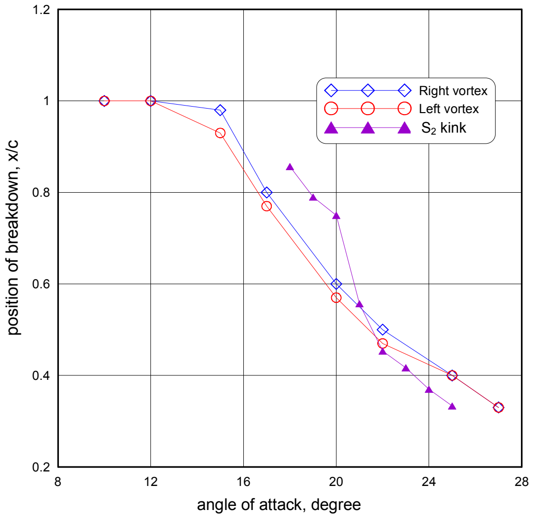

Fig. 9 Vortex breakdown and S_2 kink positions vs. angle of attack

The vortex breakdown position obtained from smoke laser sheet visualization and the S_2 kink position obtained from oil-flow visualization (U_∞ = 12 m/s) along the wing chord are shown in Fig. 9.

As is seen from the figure, there is a certain correlation between the vortex breakdown point position and the kink of the secondary vortex separation line S_2. Vortex bursting is known to lead to abrupt flow stagnation in the vortex core region and to vortex expansion. Thus, the secondary vortex is forced out to the leading edge, and the line S_2 is curved in the same direction. At $\alpha < 21°$, the S_2 kink is located downstream from the vortex core breakdown point. It is explained by the fact that the vortex breakdown phenomenon is a non-stationary process and, therefore, the vortex breakdown position migrates within certain limits. Moreover, when the dark vortex core disappears, the process of flow stagnation and vortex expansion need a certain period of time and, therefore, a certain distance before a steady burst state is reached. It is also can be noted from Fig. 9 that the motion of the vortex breakdown position upstream toward the wing tip with increasing angle of attack has an approximately linear character.

In the present study, it was assumed that the main effect of the DBD on the flow is associated with excitation of perturbations instead of acceleration of the flow in the boundary layer. Therefore, line turbulators were placed on the upper surface of the wing to find the most effective positions for flow control from the viewpoint of the maximum shift of the vortex breakdown point. The turbulators were made of a synthetic filament with a 1×1 mm square cross-section. Various turbulator configurations were tested. The most pronounced effect was observed when the turbulators were aligned perpendicularly to the wing leading edge across the vortex flow. This kind of DBD orientation was studied by Visbal and Gaitonde [10] for supersonic flow on a delta wing. The results of flow visualization with such a configuration of turbulators are illustrated in Fig. 10. It can be seen from Fig. 10a that the vortex breakdown on the right part of the delta wing without turbulators ("clear wing") occurs at x/c = 73%. Installation of two line turbulators on the right part of the wing results shifts the vortex breakdown point toward the wing tip approximately by 15% (Fig. 10b).

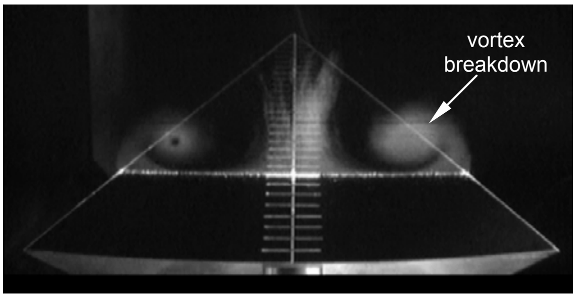

a) without turbulators (x/c = 0.73)

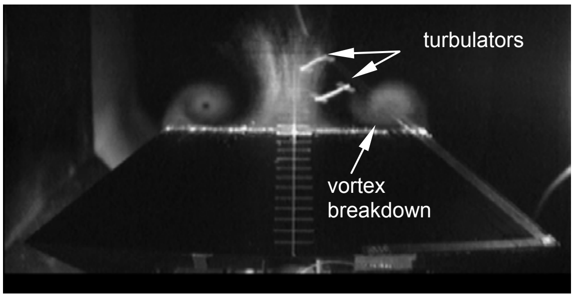

b) line turbulators on the right (x/c = 0.58)

Fig. 10 Smoke flow visualization (U_∞ = 12 m/s, α = 17°)

The surface pressure on the leeward side of the wing was measured for two cases mentioned above. The data obtained are shown in Fig. 11 as the pressure coefficient $-C_P$.

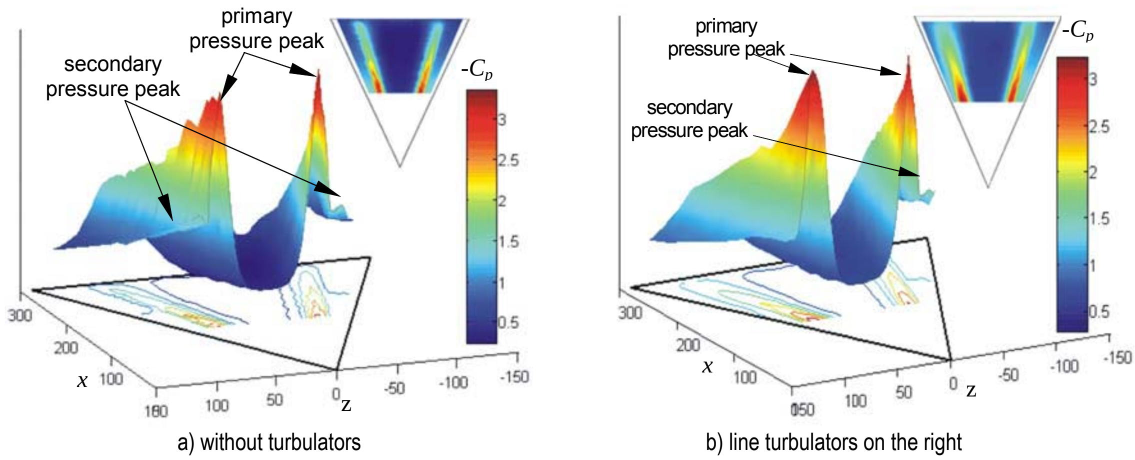

Fig. 11 Pressure coefficient distribution (U∞ = 12 m/s, α = 17°)

Fig. 11a shows that the vortex flow on the clear wing is almost symmetrical, which is manifested in identical widths of the pressure peaks generated by the primary vortices. Moreover, two pressure peaks of lower intensity generated by the secondary vortices are clearly observed on both the left and the right parts of the wing. Installation of turbulators as described above makes the right primary pressure peak wider due to breakdown of the right primary vortex (Fig. 11b). Only one secondary pressure peak is observed on the left part of the delta wing in this case (Fig. 11b). The absence of the secondary pressure peak on the right side has the same explanation as that given earlier in the case of oil-flow visualization. When the primary vortex breaks down, its core diameter increases, thus, forcing out the secondary vortex closer to the wing leading edge. It can be seen from the figure that the suction peak on the right side has the same order of magnitude as the left one for the case of the clear wing. The -C_P peaks decay in the downstream direction with the same ratio for both halves of the model. In the case of the wing with turbulators on the right side, the decay ratio on the right is higher than on the left side and in the case of the clear wing.

As the design of DBD electrodes is simple, the experiments on DBD-assisted vortex flow control were carried out with different configurations of DBD actuators. The first configuration is shown in Fig. 12. DBD actuators installed in the same manner as turbulators were found to ensure the most effective vortex breakdown control. In this case, the DBD electrodes were perpendicular to the leading edge. The distances between the exposed electrodes were 30 mm. The electrodes were arranged to generate flow acceleration toward the wing tip. The experiments were performed in the range of velocities U_∞ = 10 ÷ 30 m/s at α = 10° ÷ 25°. Fig. 12 shows an example of the vortex flow pattern in the laser sheet plane with and without DBD excitation.

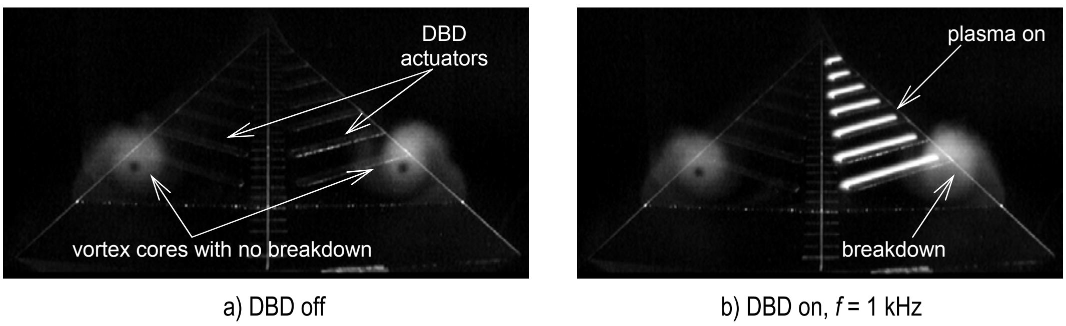

Fig. 12 Smoke flow visualization (view from the trailing edge), U∞ = 12 m/s, α = 15°

It is seen from Fig. 12a that there are two vortices with well-defined dark cores on the left and right sides of the wing in the “DBD off” case. If the DBD is activated on the right part of the wing (Fig. 12b), only the

left vortex has a core, while the right one is destroyed.
The next DBD configuration is shown in Fig. 13. In this case, the DBD actuator was placed along the secondary separation line (see Fig. 7) on the leeward side of the wing. Here, the DBD actuator was assumed to affect the shear layer between the primary and secondary vortices due to insertion of mass flow and, probably, acoustic disturbances and cause vortex breakdown. Actually, the data obtained show that such a configuration was ineffective from the viewpoint of vortex breakdown. Further experiments with a configuration where the DBD operation parameters (voltage and frequency) were varied, however, revealed that the DBD can not only lead to vortex bursting but also to vortex stabilization. The data obtained in these experiments are shown in Fig. 13.

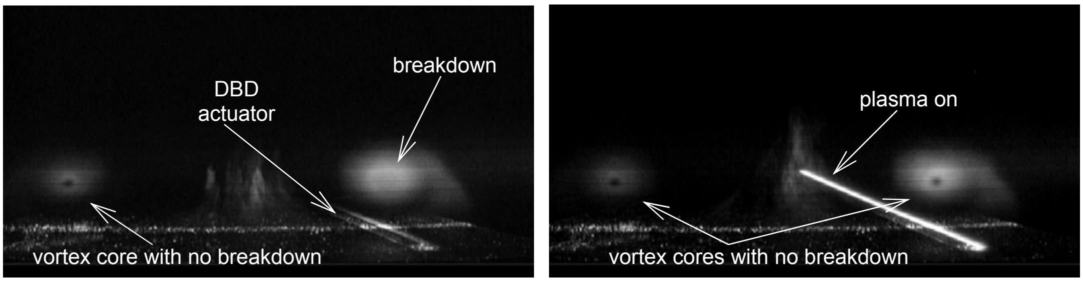

a) DBD off b) DBD on, f = 1.6 kHz, F=50 Hz

Fig. 13 Smoke flow visualization (view from trailing edge), U_∞ = 7 m/s, α = 15°

As is seen from Fig. 13a, in the “DBD off” case, only the left vortex has a dark core, while the right vortex is destroyed. If the DBD is activated on the right part of the delta wing, both vortices have well-defined dark cores (Fig. 13b). In other words, DBD activation leads to vortex stabilization on the right part of the wing. It should be noted that the effect of vortex stabilization was achieved under certain conditions: DBD operation in the burst mode. The effect was observed only in a narrow range of burst parameters, namely, if the pulse packet repetition frequency was 50 Hz.
For the configurations mentioned PIV measurements were performed. Sections of measurements were defined basing on data of laser sheet visualization. Measurement regions were chosen to cover leading edge of the model and zone of primary vortex on the right part of delta wing.
It was obtained that excitation of the flow by the first kind of actuator (see Fig. 12) results in vortex breakdown on the right part of the model. Velocity and vorticity distributions measured in the section x/c = 0.75 are presented in Fig. 15 - Fig. 15.

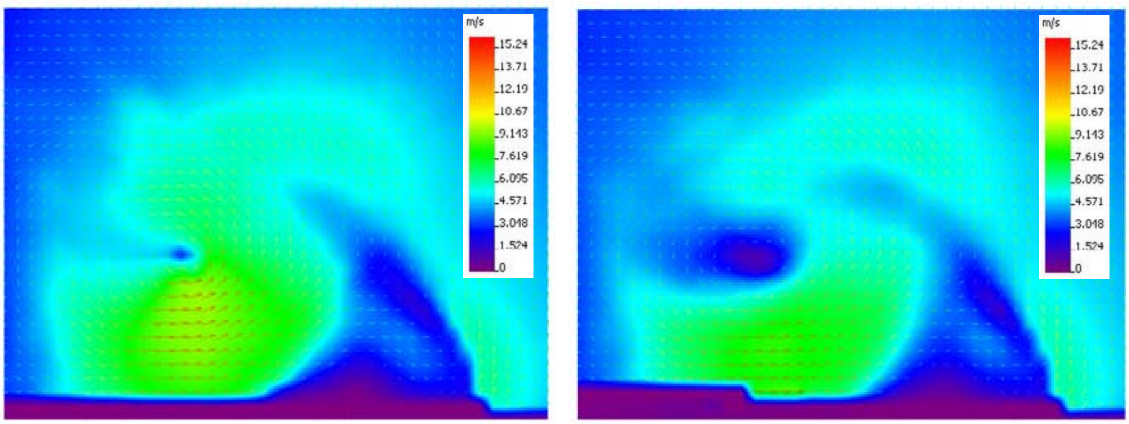

a) DBD off b) DBD on

Fig. 14 Velocity distribution for excitation in variant 1 (a =15° , U_∞ = 7 м/с,
left – no excitation, right – continuous excitation f = 1.6 kHz)

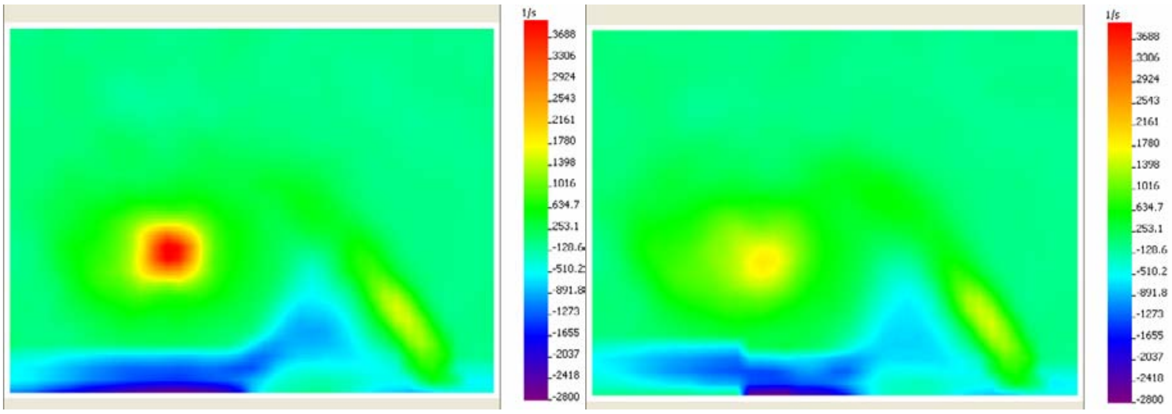

a) DBD off b) DBD on

Fig. 15 Vorticity distribution for excitation in variant 1 *(a =15° , U_∞ = 7 м/с,*
left – no excitation, right – continuous excitation f = 1.6 kHz)

These data were obtained by averaging of 500 instantaneous fields. Core of the primary vortex can be easily defined on the figures. Resolution of PIV is sufficient to resolve secondary separation and vortex near the leading edge. Core of the primary vortex is well pronounced in Fig. 15a - Fig. 15a and smeared in Fig. 15**Ошибка! Источник ссылки не найден.**b - Fig. 15b due to vortex breakdown upstream for the case of active DBD. It can be seen from the figures that downstream of breakdown point vorticity in the vortex core and also induced circular velocity suddenly decrease. This leads to decreasing of suction on the model surface as it was shown above.

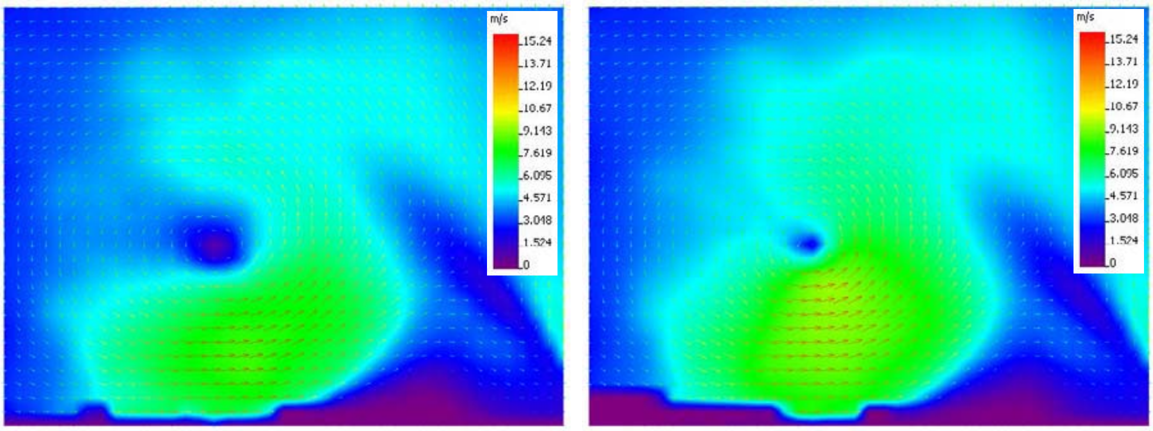

a) DBD off b) DBD on

Fig. 16 Velocity distribution for excitation in variant 2 *(a =15° , U_∞ = 7 м/с,*
left – no excitation, right – continuous excitation f = 1.6 kHz)

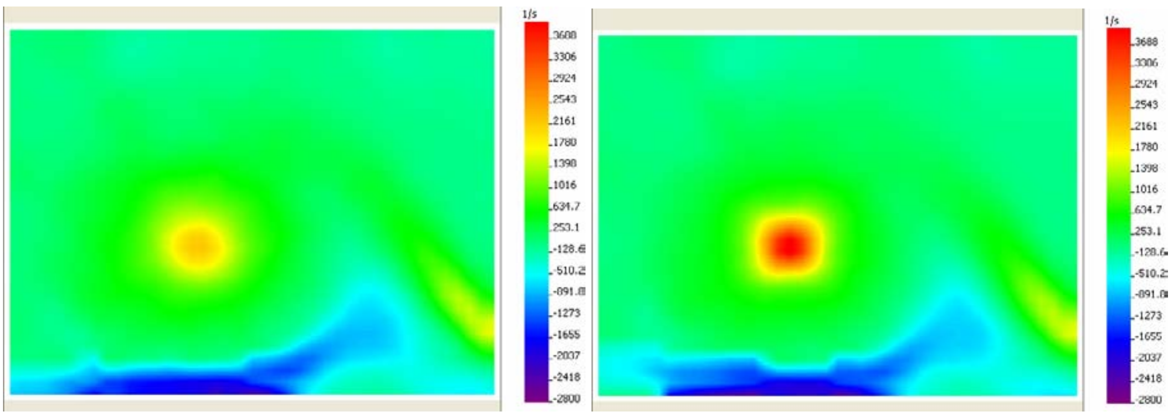

a) DBD off b) DBD on

Fig. 17 Vorticity distribution for excitation in variant 2 *(a =15° , U_∞ = 7 м/с,*
left – no excitation, right – continuous excitation f = 1.6 kHz)

Data obtained for the second electrode configuration are presented in Fig. 16 - Fig. 17. The section of measurements was chosen downstream of natural breakdown point. It can be seen from the figures that the vortex core recovers and circular velocity increases for the case of active DBD. The effect obtained is probably connected with stabilization of the secondary separation line that leads to stabilization of the whole flow and damping of pulsations. As a result later vortex breakdown was obtained in the experiment.

Conclusions

The possibility of vortex flow control on the model of a delta wing was studied at a subsonic speed in the range of chord-based Reynolds numbers $0.06 \div 0.7 \cdot 10^6$. Dielectric barrier discharge plasma on the model surface was used for vortex breakdown control. The effects of the angle of attack of the model, discharge operating parameters, and location and geometry of DBD actuators were studied in the experiments. It was found that DBD is able not only to influence the vortex breakdown position but also lead to vortex stabilization when operating in the burst mode. Thus, it was demonstrated that the DBD can be successfully applied for vortex flow control on a delta wing at high angles of attack. The experimental results showed that variations of DBD location, power, and frequency exert a significant effect on the vortex breakdown control efficiency. The highest efficiency from the viewpoint of vortex breakdown was reached with the DBD placed perpendicularly to the leading edge across the vortex flow. The configuration with DBD actuators aligned along the secondary separation line proved to be most effective from the viewpoint of vortex stabilization.

Acknowledgements

This work was supported by the ISTC project #3646 and was devoted to the memory of AIAA Fellow Norman D. Malmuth .

References

[1] William H. Wentz and David L. Kohlman., “Wind Tunnel Investigations of Vortex Breakdown on Slender Sharp-Edged Wings,” Technical Report FRL 68-013, University of Kansas Center for Research, Inc., 1968.

[2] Mabey D.G., “Similitude Relations for Buffet and Wing Rock on Delta Wings,” Progress in Aerospace Sciences, Vol. 33, No. 7, 1997, pp. 481-511(31)

[3] Roth, J. R., Wilkinson, Stephen P. “Boundary Layer Flow Control with a One Atmosphere Uniform Glow Discharge Surface Plasma,” AIAA-1998-328 Aerospace Sciences Meeting and Exhibit, 36th, Reno, NV, Jan. 12-15, 1998

[4] J. Reece, Roth and Xin, Dai, “Optimization of the Aerodynamic Plasma Actuator as an Electrohydrodynamic (EHD) Electrical Device,” AIAA Paper 2006-1203, 2006.

[5] Corrie Baird, C. L. Enloe, Thomas E. McLaughlin, and James W. Baughn, “Acoustic Testing of the Dielectric Barrier Discharge (DBD) Plasma Actuator,” AIAA Paper 2005-565, 2005.

[6] Post, M., and Corke, T., “Separation Control on High Angle of Attack Airfoil Using Plasma Actuators,” AIAA Paper 2003-1024, 2003.

[7] Post, M., and Corke, T., “Separation Control Using Plasma Actuators - Stationary and Oscillating Airfoils,” AIAA Paper 2004-0841, 2004.

[8] Anatoly Maslov, Andrey A. Sidorenko, Boris Yu. Zanin, Boris V. Postnikov, Alexey D. Budovsky and Norman D. Malmuth, “Plasma Control of Flow Separation on Swept Wing at High Angles of Attack,” AIAA Paper 2008-540, 2008.

[9] Zverkov, I., Zanin, B., and Kozlov, V, “Investigation of Disturbances Growth in Boundary Layers on Classical and Wavy Surface Wings,” AIAA J. Vol. 46, No. 12, 2008, pp. 1023-1033.

[10] Visbal, M. R., and Gaitonde, D. V., “Control of Vortical Flows Using Simulated Plasma Actuators,” AIAA Paper 2006-505, 2006.